SLAC-PUB-12239
January 2007
(A)

Start-to-end beam optics development and multi-particle tracking for the ILC undulator-based positron source*

F. Zhou, Y. Batygin, Y. Nosochkov, J. C. Sheppard, and M. D. Woodley

Stanford Linear Accelerator Center, 2575 Sand Hill Road, Menlo Park, CA 94025, USA

Abstract

Undulator-based positron source is adopted as the ILC baseline design. Complete optics to transport the positron beam having large angular divergence and large energy spread from an immersed thin Ti target to the entrance of the 5 GeV damping ring injection line is developed. Start-to-end multi-particle tracking through the beamline is performed including the optical matching device, capture system, transport system, superconducting booster linac, spin rotators, and energy compressor. It shows that 49.8% of the positrons from the target are captured within the damping ring 6-D acceptance – $A_x + A_y \le 0.09\,\mathrm{m}$ and $\Delta E \times \Delta z \le (\pm 25\mathrm{MeV}) \times (\pm 3.46\mathrm{cm})$ – at the entrance of the damping ring injection line. The field and alignment errors and orbit correction are analyzed.

* Work supported by DOE contract DE-AC02-76SF00515

Start-to-end beam optics development and multi-particle tracking for the ILC undulator-based positron source

F. Zhou, Y. Batygin, Y. Nosochkov, J. C. Sheppard, and M. D. Woodley

Stanford Linear Accelerator Center, 2575 Sand Hill Road, Menlo Park, CA 94025, USA

Abstract

Undulator-based positron source is adopted as the ILC baseline design. Complete optics to transport the positron beam having large angular divergence and large energy spread from an immersed thin Ti target to the entrance of the 5 GeV damping ring injection line is developed. Start-to-end multi-particle tracking through the beamline is performed including the optical matching device, capture system, transport system, superconducting booster linac, spin rotators, and energy compressor. It shows that 49.8% of the positrons from the target are captured within the damping ring 6-D acceptance – $A_x + A_y \le 0.09\,\mathrm{m}$ and $\Delta E \times \Delta z \le (\pm 25\mathrm{MeV}) \times (\pm 3.46\mathrm{cm})$ – at the entrance of the damping ring injection line. The field and alignment errors and orbit correction are analyzed.

1. Overview

The undulator-based positron source is adopted as the International Linear Collider (ILC) baseline design, which uses a ~100-m-long helical undulator (K≈1, λ≈1 cm) placed at the 150 GeV point of the ILC electron main linac. The 150 GeV ILC electron beam passing through the undulator generates circularly polarized photons, which impinge on an immersed Ti target with thickness of 0.4 radiation length and produce longitudinally polarized positrons. The generated positron beam will be first collected and accelerated to 125 MeV. Then a dogleg is used to separate positrons from electrons and photons. Positrons are accelerated to 400 MeV in the normal conducting pre-acceleration linac. The 400 MeV beam passes through a beamline to the electron main linac tunnel, along which the beam travels for 4.1-km. Then the positron beam is transferred from the electron main linac tunnel to the positron booster linac tunnel through a beamline, and continues to pass through a 479 m of beamline up to the superconducting positron booster linac. After acceleration to 5 GeV, it is transported from the booster linac to ring performing the spin rotations and energy compression, and finally injecting into the damping ring (DR) injection line. The overall optics and geometry of the positron source are shown in Figs. 1 and 2, respectively.

This technical note is organized as follows: the optics for each part of the beamline is described in section 2; section 3 presents the start-to-end multi-particle tracking without and with magnet errors and orbit correction; and, finally, the results are summarized in section 4.

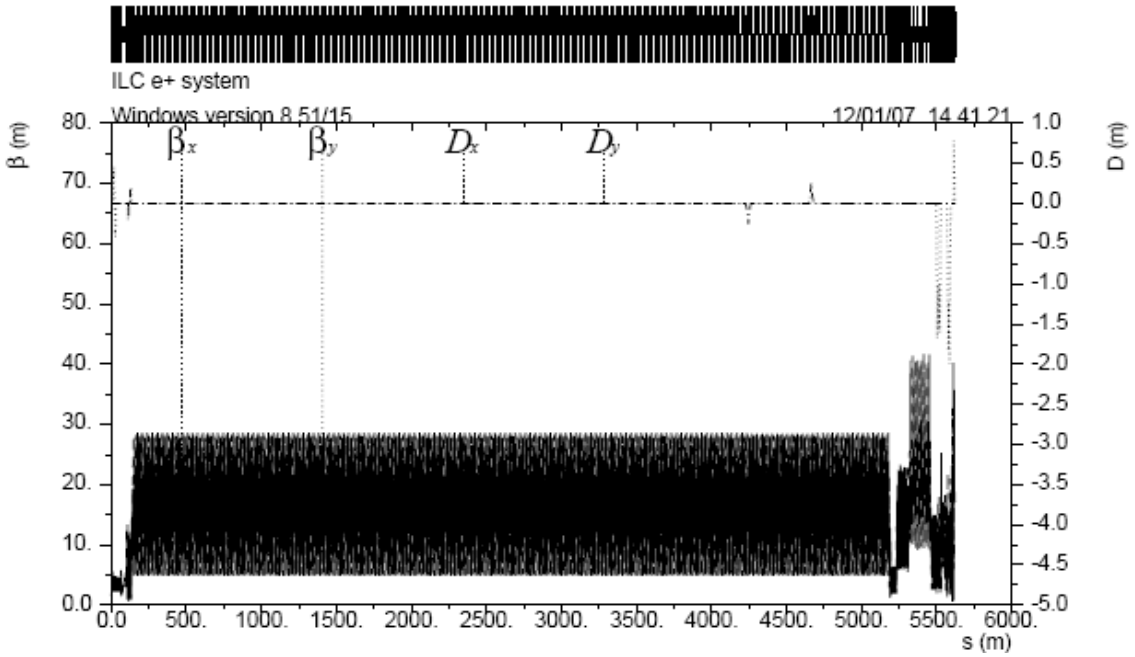

FIG.1. Overall optics of the positron source.

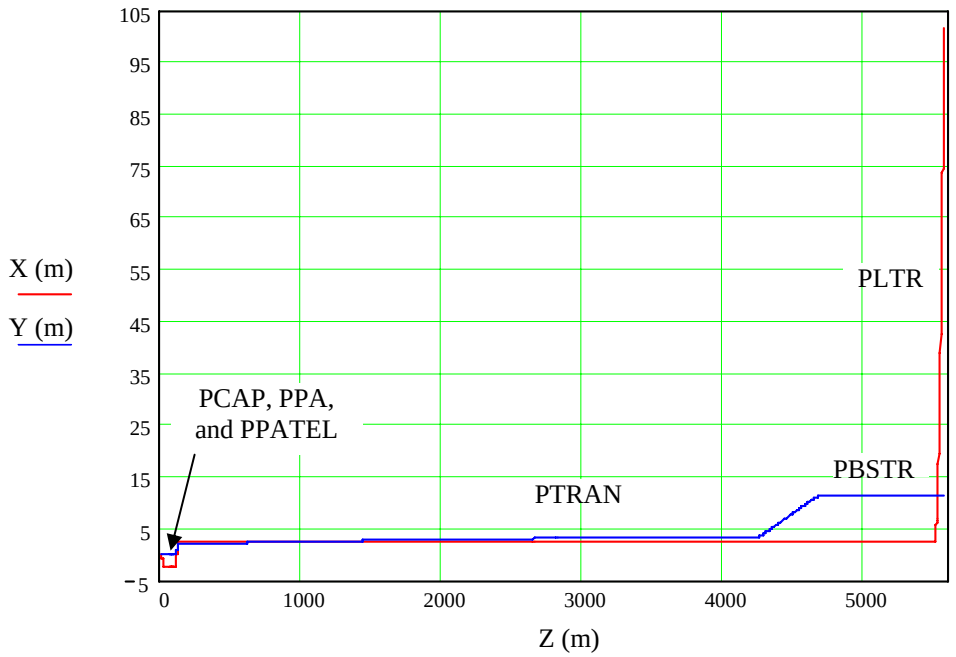

FIG. 2. Overall geometry of the positron source.

2. Start-to-end optics developments

The positrons emerging from a thin Ti target are collected and accelerated in a beamline named as Optical Matching Device (OMD) and pre-acceleration capture system. The OMD is used to transform positrons characterized by small spot size and large divergence at the target into small angular divergence and large size to match pre-acceleration capture system consisting of normal conducting L-band RF structures embedded in a solenoid. It is a tapered solenoid from 6 T on the target to 0.5 T on the L-band structures. The optimum on-axis field distribution for the matching device needs to obey: $B(z) = B_0/(1+g\cdot z)$, where B_0 is the magnetic field on the target, g is the taper parameter, and z is the longitudinal coordinate. The condition for an adiabatic field variation is given by $gP/(eB_0) << 1$ (P is particle momentum); to fulfill the condition for particles with higher energy the taper parameter g should be small. However, the small g means that the matching section becomes long, and thus the bunch lengthening becomes stronger [1]. Parameter optimizations in the OMD and the capture cavities are described in detail in Ref. [2]. The positrons are accelerated to 125 MeV through the pre-acceleration capture system.

2.1 Optics of the PCAP, PPA, and PPATEL

The positrons following the capture system are transported by the "Positron CAPture" beamline (PCAP), which separates positrons from electrons and photons by using a dogleg with a horizontal offset of 2.5 m. The collimators to scrape the positrons with large incoming angles and large energy errors are installed. The optics details can be found in [3].

The "Positron Pre-Accelerator" beamline (PPA) immediately downstream of the PCAP is used to accelerate positrons from 125 MeV to 400 MeV. It consists of the normal conducting L-band RF structures [4] embedded in a constant solenoid field of 0.5 T. The MAD code does not have an element containing RF structure embedded in a solenoid, but one can use an approximate model in the MAD by longitudinally slicing both the RF structures and the solenoid, and alternating these slices for a smooth effect of both the RF and solenoid field. In this model, the solenoid field B_z in each slice is constant, but the solenoid strength $K_s = B_z/(B\rho)$, where $B\rho$ is the magnetic rigidity, varies from slice to slice with the beam energy. For an accurate model, the number of RF and solenoid slices must be sufficiently large. The optics calculation with this model does agree well with PARMELA calculation, which can directly model RF structures embedded in a solenoid. The accelerating gradient of the L-band structure in the PPA system is 8.0 MV/m, and about 34.6 m of the PPA length is required to accelerate the beam to 400 MeV.

The beamline named as "Positron Pre-Accelerator To the Electron main Linac tunnel" (PPATEL), is to transport the 400 MeV beam from the PPA to the electron main linac tunnel. It uses a horizontal and vertical dogleg to deflect the beam by 5 m and 2 m in the horizontal and vertical planes, respectively. As a result, the positron line at exit of the PPATEL is positioned 2 m high and exactly on top of the electron main linac beamline. The optics details can be found in Ref. [3].

Figs. 3 and 4 show the optics and geometry of the PCAP, the PPA, and the PPATEL system, respectively.

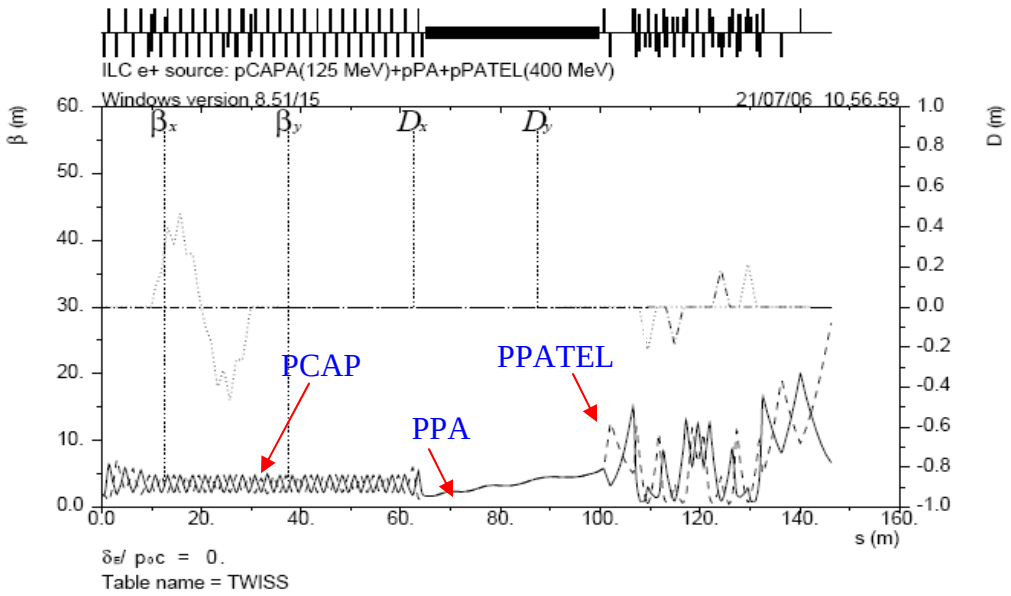

FIG. 3. Optics of the PCAP, the PPA, and the PPATEL.

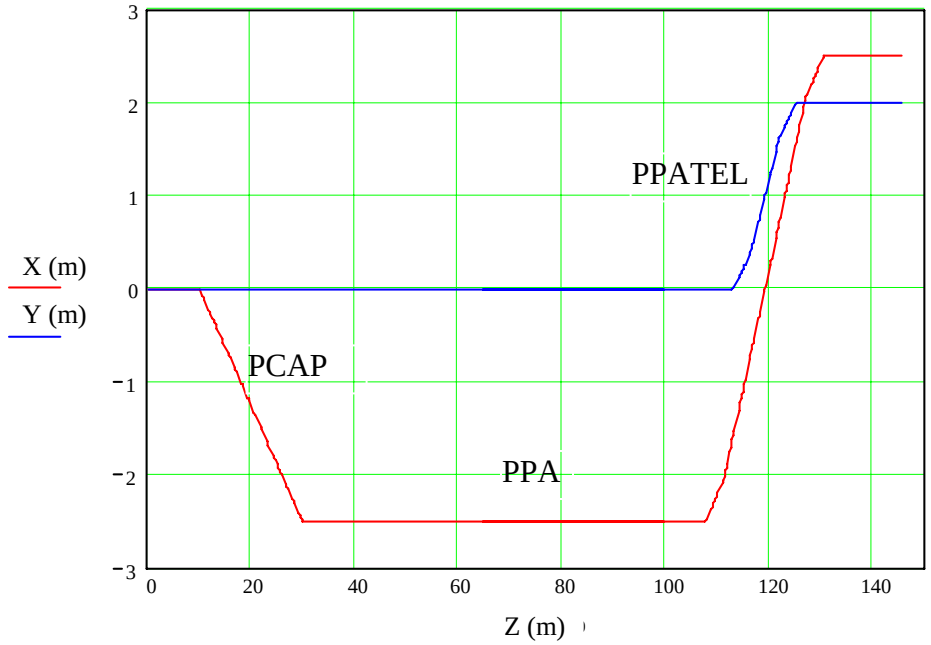

FIG. 4. Geometry of the PCAP, the PPA, and the PPATEL.

2.2 Optics of the PTRAN system

In the ILC positron source baseline design, the Positron TRANsport (PTRAN) system was ~18 km long used to bring positrons from the electron main linac side to the positron main linac side bypassing the interaction point, from the end of the PPATEL to the entrance of the Trombone system used for path length adjustments [5]. In September 2006, after the Vancouver Global Design Effort meeting, the ILC layout was changed to central DRs based complex, where the PTRAN system only needs about 5.03 km length and the Trombone system was removed. The PTRAN system has three sections: PTRANa – to deliver positrons on the top of the electron main linac for 4.09 km; PTRANb - to transfer positrons from the electron main linac tunnel to the positron booster linac tunnel through a 462 m of beamline; and PTRANc - to transport positrons through a 479 m of beamline up to the positron booster linac. The PTRAN system uses standard FODO cells, each of which is 16.8 m long. Phase advance per cell is 90° and maximum β-function is ~28.5 m. The PTRANa follows the earth curvature as does the main linac tunnel. To simulate the beam to follow the curvature, presently a tiny vertical bend is used in each cell, whose bending angle is $16.8/(6378\times10^{3}) = 2.63$ μrad. It generates ~0.08 mm of the dispersion along the PTRANa. Positron tracking shows that the small dispersion does not degrade the beam performance since the dispersion contribution to the beam size is negligible compared to the beam size due to the large emittance. In the real machine, no dispersion should be generated for that matter, which can be modeled by implementing the solution developed in Ref. [6]. The PTRANb – a vertical dogleg - is to provide 8 m of vertical offset to bring the positron beam from the electron main linac tunnel to the positron booster linac tunnel. On both ends of the PTRANb a double bend achromat is used to provide 19.0 mrad of the bending angle. Four quadrupoles are inserted in between the two bends so that the phase advance between the two bends is 180° and the dispersion is thus cancelled. 479 m of the PTRANc is to connect the positron booster linac with PTRANb. The optics and geometry of the whole PTRAN system are shown in Figs. 5 and 6, respectively.

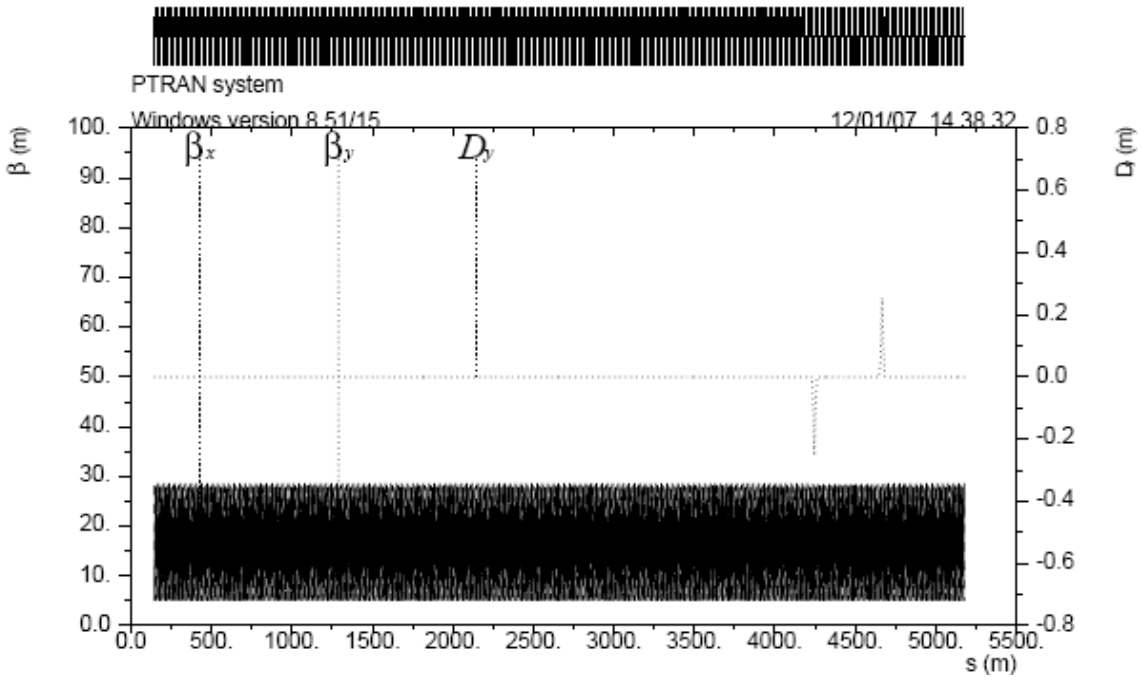

FIG. 5. Optics of the PTRAN system.

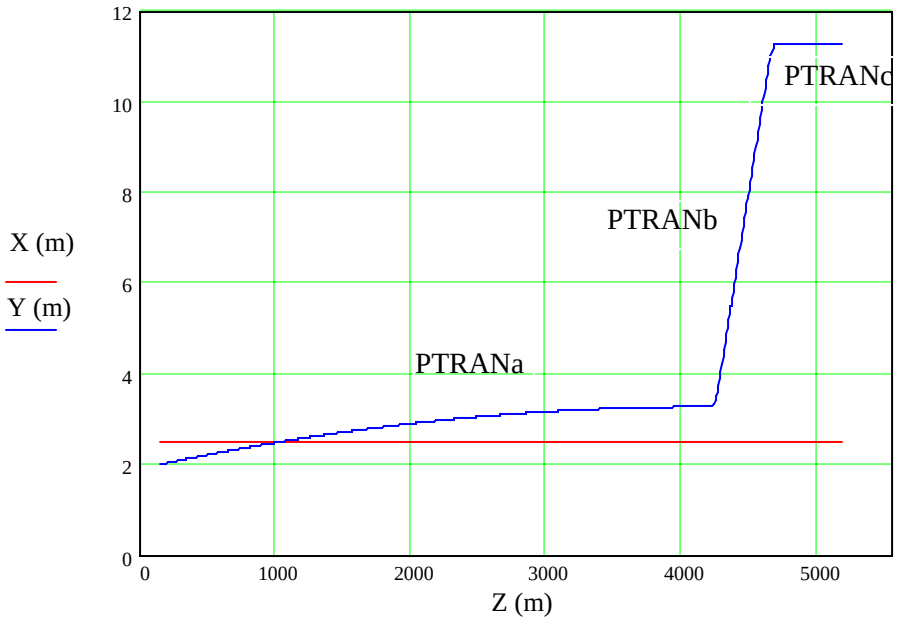

FIG. 6. Geometry of the PTRAN system.

2.3 Optics of the PBSTR system

The Positron BooSTeR linac (PBSTR) starts from the end of the PTRAN beamline and accelerates the beam from 400 MeV to 5 GeV through the superconducting L-band Cryo-modules. The PBSTR has three sections. The energy in the first section ranges from 400 MeV to 1083 MeV, and four non-standard-ILC-type cryomodules are used, each of which has six 9-cell cavities and six quadrupoles. Typical FODO cells are used, and the field strength of quadrupoles, $(\partial B/\partial x)\times L$, is in range of 0.88-2.0 T. In the second section, the beam energy increases from 1083 MeV to 2626 MeV, and six standard ILC-type cryomodules are used, each of which has eight 9-cell cavities and two quadrupoles. $(\partial B/\partial x)\times L$ is in the range of 0.62-1.3 T. Finally, the positrons are accelerated to 5 GeV using twelve standard ILC-type cryomodules, each of which has eight 9-cell cavities and one quadrupole. And $(\partial B/\partial x)\times L$ is in the range of 0.95-1.63 T. The optics of the PBSTR system is shown in Fig. 7.

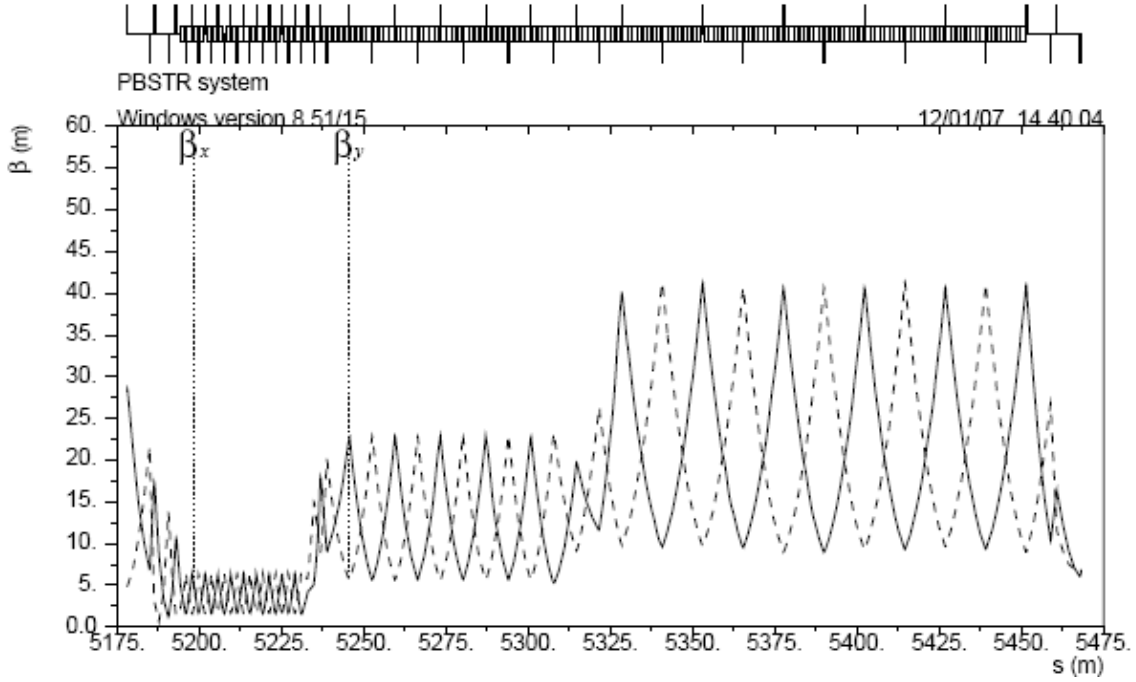

FIG. 7. Optics of the PBSTR system.

2.4 Optics of the PLTR system

The Positron Linac-to-Ring (PLTR) system, which extracts the positrons from the PBSTR system and injects them into the DR injection line, has two main functions: one is to rotate the positron spin vector to the vertical plane; and the other is to manipulate energy compression to meet the DR longitudinal acceptance. The longitudinal polarization of the positrons is generated at the target and preserved prior to the DR. In the DR, only positron spin directions parallel or anti-parallel to the magnet field – that is,

transverse to the plane of the DR – will preserve their polarization. The PLTR system consists of bending magnets and solenoid that change the spin of positrons first from the longitudinal to horizontal plane and then from the horizontal to the vertical, parallel to the magnetic field of the DR (the magnetic field in the DR is in the vertical plane). The spin precession with respect to the momentum vector caused by a bending angle, θ_{bend}, is given by:

$$\theta_{spin\_bend} = \frac{E(GeV)}{0.44065} \cdot \theta_{bend} \quad , \tag{1}$$

where E is the positron energy. Rotation of the spin vector in the horizontal plane by $n \cdot 90°$ (n is an odd integer) from the longitudinal direction requires a total bending angle of $\theta_{bend} = n \cdot 7.929°$ at 5 GeV. When a positron passes through a solenoid, its component of spin perpendicular to the solenoid field is rotated around the solenoid field axis. The rotation angle is approximately twice the rotation angle of the positron trajectory. The spin rotation angle caused by a solenoid is thus given by:

$$\theta_{spin\_sole} \approx \frac{B_z \cdot L_{sole}}{B\rho} \quad , \tag{2}$$

where B_z is the longitudinal solenoid magnetic field, L_{sole} is the solenoid length, $B\rho$ is the magnetic rigidity. For a 90° of spin rotation from the horizontal to the vertical plane at 5 GeV, a solenoid magnetic field integral of $B_z \times L_{sole}$ = 26.23 T.m is needed. An 8.3-m-long superconducting solenoid with B_z =3.16 T is used.

The bunch decompression or energy compression can be realized by properly manipulating the linac RF phase with a suitable transfer function, $R_{56} = \int \frac{D_x}{\rho} ds$ (D_x is the dispersion, ρ is the bending radius), generated in bends:

$$\Delta z \approx R_{56} \cdot \frac{dp}{p} + T_{566} \cdot \left(\frac{dp}{p} \right)^2 \quad , \tag{3}$$

where $\frac{dp}{p}$ is the induced correlated energy spread and T_{566} is the second order term of transfer matrix. The first LTR arc having four FODO cells inserted with 8 bends is designed for the energy compression and spin rotation. A bending angle of $7 \times 7.929° = 55.5°$ is chosen in the design. The nominal R_{56} is 86 cm but adjustable within the range of ±30cm. After the bunch decompression, an RF voltage of 180 MV provided by a 6-m-long superconducting linac is implemented to rotate the positrons in the longitudinal phase space to match the DR longitudinal acceptance.

The rest of the PLTR system includes: a section to have an additional 34.5° horizontal bending, and a matching section with 4 quadrupoles and a double bend achromat used to

match Twiss parameters at the DR injection line [7]. Its optics and geometry are shown in Figs. 8 and 9, respectively.

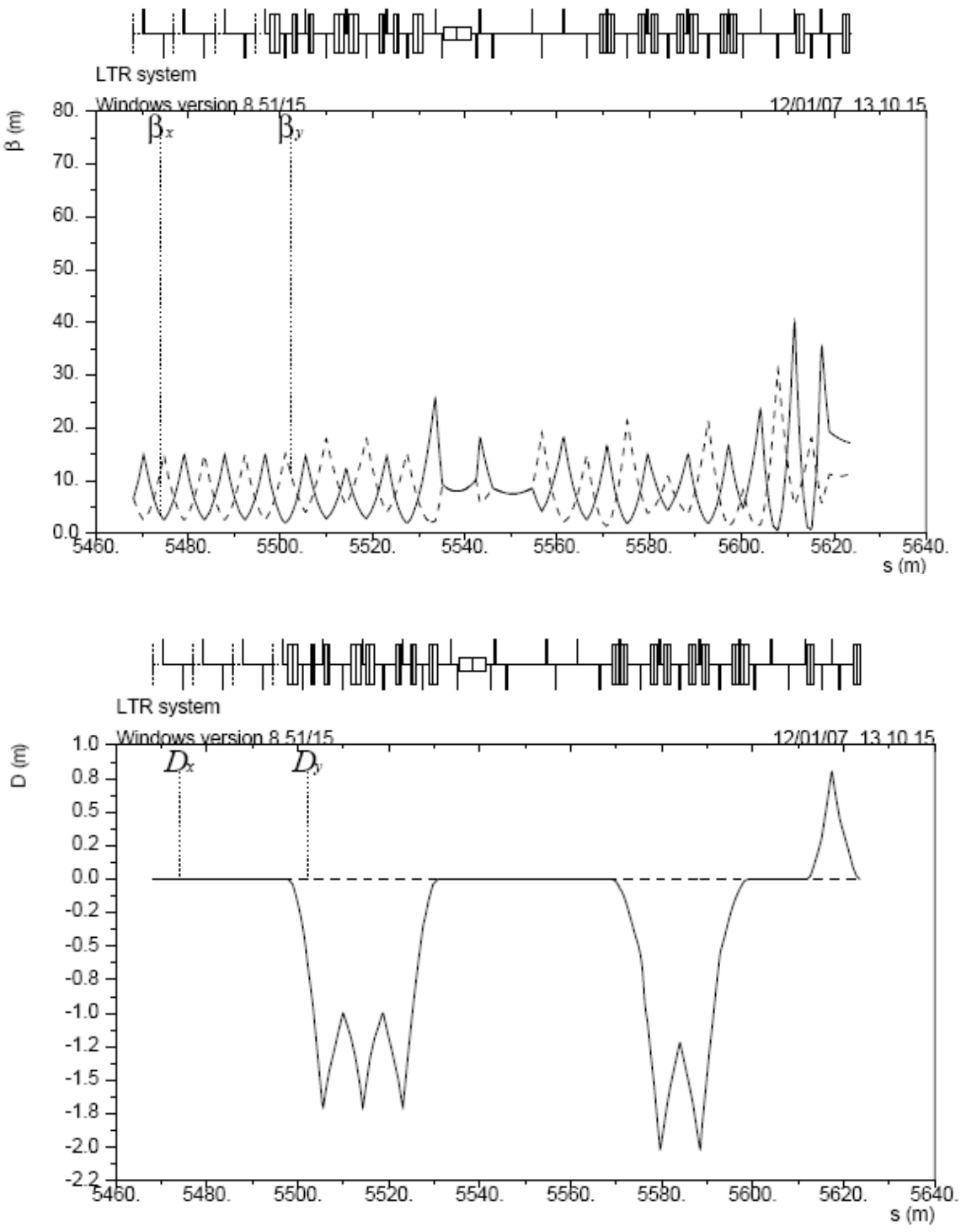

FIG. 8. PLTR β functions (top) and dispersion (bottom).

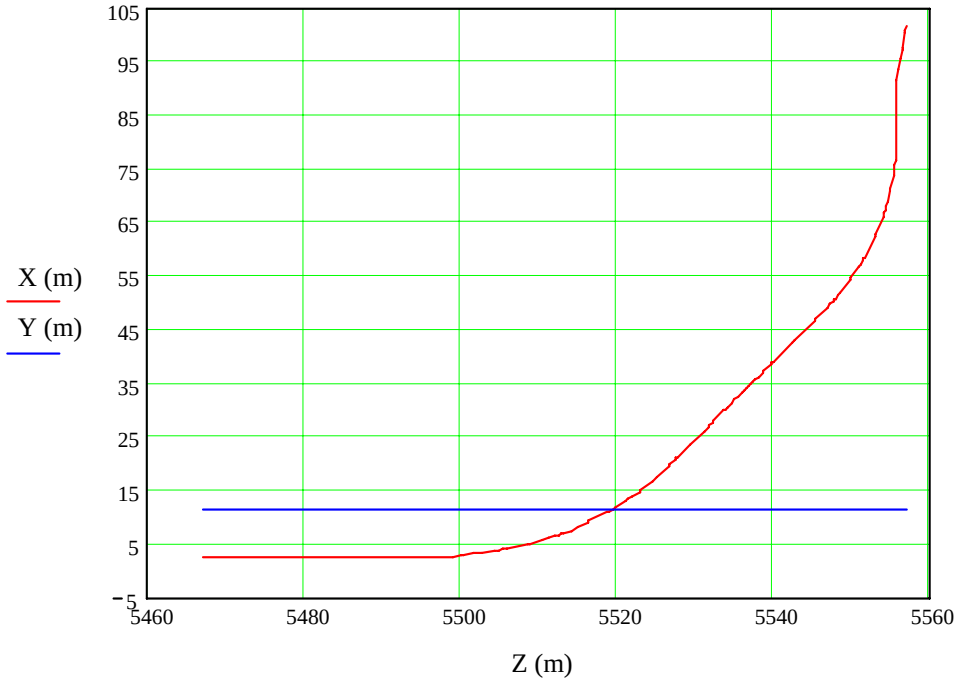

FIG. 9. Geometry of the PLTR system.

2.5 Emittance measurement, PPS stoppers, and 5-GeV beam dump

The 5-GeV beam emittance is measured using wire scanners located at the standard FODO cells immediately downstream of the PBSTR. Three Personal Protection System (PPS) stoppers with 1-m in each are installed in the drifts in between the bends and quadrupoles of the first LTR arc. A 5-GeV beam dump is located downstream of the emittance measurement station. To dump a 5 GeV beam, the first bend in the PLTR needs to be turned off. The dump line, shown in Fig. 10, includes a defocusing quadrupole, a dump bend, a 0.8-m long focusing quadrupole, and a 9.1-m long drift to the dump window. At the dump window, for ±0.1% and ±10% of energy spread, the half edge beam sizes $\sigma x/\sigma y$ are 3.9 cm/8.3 cm and 14.3 cm/8.3 cm, respectively, which meet the dump window specifications [8]. At the monitor location shown in Fig. 10, the dispersion dominates the beam size, and thus the dump line can be used as an energy spectrometer with ~0.1% of resolution.

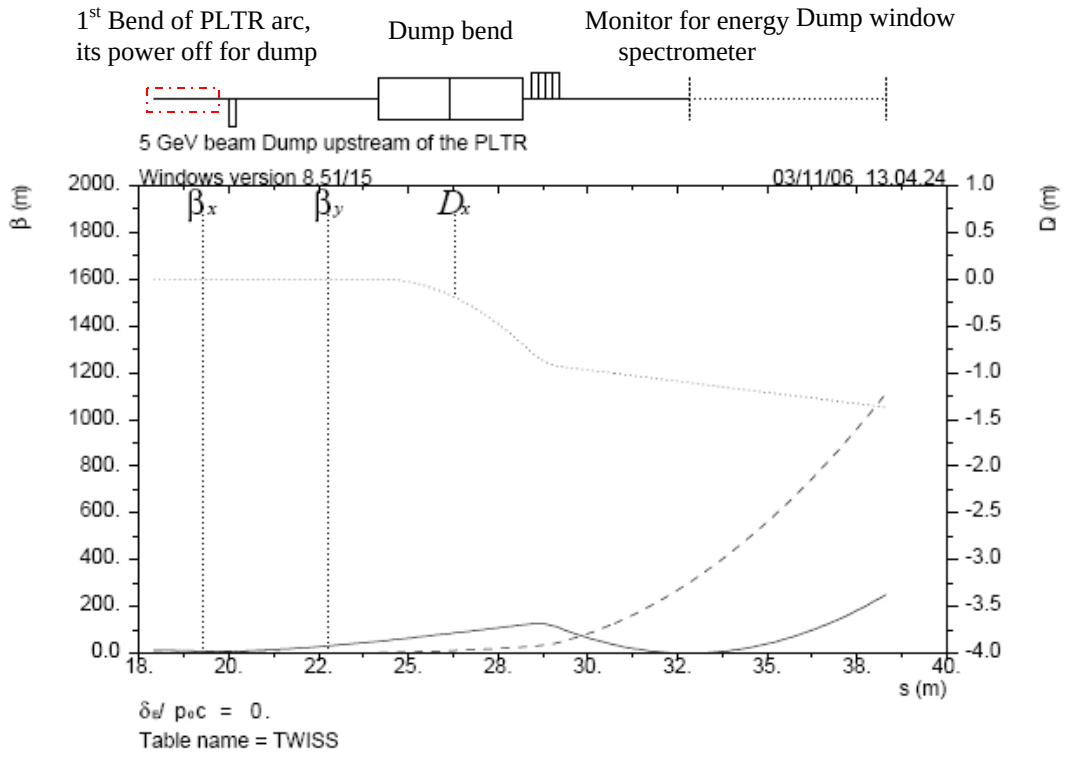

FIG. 10. 5 GeV beam dump line downstream of the PBSTR system.

3. Multi-particle tracking from the immersed thin target to the entrance of the DR injection line

3.1 Tracking without magnet errors

Multi-particle tracking from the immersed thin Ti target to the entrance of the DR injection line has been performed. The tracking from the target to the capture cavities (125 MeV) is described in detail in Ref. [2], and the 6-D coordinates at the capture cavities exit are shown in Fig. 11. The ELEGANT code [9] is then used to track the positron beam through the rest of the positron beamline including the PCAP, the PPA, the PPATEL, the PTRAN, the PBSTR, and finally the PLTR system. Positron 6-D coordinates at the exit of the capture cavities are used as the input data in the ELEGANT code tracking. To accommodate more positrons within the DR 6-D acceptance – $A_x + A_y \leq 0.09\,\mathrm{m}$ and $\Delta E \times \Delta z \leq (\pm 25\mathrm{MeV}) \times (\pm 3.46\mathrm{cm})$ [10], the energy compression is optimized in the PLTR before injecting into the DR injection line. For that purpose, the PBSTR upstream of the PLTR runs booster linac RF phase off-crest to create a suitable correlated energy spread. Fig. 12 shows the longitudinal phase space at the PLTR exit after energy compression. Tracking shows that 55.4% of positrons from the target can survive the transport through the complete beamline based on the physical apertures of the beam pipes listed in Table I. Positron loss distribution along the beamline is shown in Fig. 13. Some positrons survived in the beamline, however, may not be captured within

the DR acceptance. To calculate positrons capture efficiency within the DR 6-D acceptance, first we calculate the twiss parameters α, β, and γ from the beam distribution. In the x-plane, these parameters are given by:

$$\alpha_x = -\frac{\langle x \cdot x' \rangle}{\varepsilon_x},\ \beta_x = \frac{\langle x^2 \rangle}{\varepsilon_x}, \text{ and } \gamma_x = \frac{\left(1+\alpha_x{}^2\right)}{\beta_x},$$

where the un-normalized rms emittance is $\varepsilon_x = \sqrt{\langle x^2 \rangle \langle x'^2 \rangle - \langle x x' \rangle^2}$. Parameter calculations for α_y, β_y, and γ_y in the y-plane are analogous to the x-plane. Twiss parameters α_x (α_y), β_x (β_y), and γ_x (γ_y) define a family of ellipses with the same ratio of semi-axes. For particles with index *i*, its un-normalized emittance

$$\varepsilon_{x,i} = \gamma_x \cdot x_i^{\,2} + 2\alpha_x \cdot x_i \cdot x_i' + \beta_x \cdot x_i'^2 \qquad ,$$

and $\varepsilon_{y,i}$ is calculated analogously. Given the normalized transverse emittance, $\gamma_{i,energy} \cdot (\varepsilon_{x,i} + \varepsilon_{y,i}) \le 0.09\,\text{m}$, where $\gamma_{i,energy}$ is the Lorentz factor for the particles with index *i*, and the longitudinal phase space is within the DR acceptance, the particle is considered captured. Without the PLTR, the tracking shows that only 32.3% of positrons from the target are captured within the DR 6-D acceptance. With the PLTR energy compression, 49.8% of the positrons from the target are captured within the DR 6-D acceptance at the entrance of the DR injection line. Therefore, out of 55.4% survived positrons, 5.6% positrons are beyond the DR 6-D acceptance. An energy collimator is first considered to be installed in the second arc of the PLTR to scrape these unwanted positrons; its length is 10 cm, and the half apertures in x- and y- plane is 1.4 cm and 3.5 cm, respectively. With the collimator, unwanted positrons reaching the DR are reduced from 5.6% to 1.1%, as shown in Fig. 13, and the positrons within the DR acceptance are also decreased from 49.8% to 48.4% due to the collimation. The phase space with the collimation is shown in Fig. 14. Additional betatron and energy collimators may be required to collimate the rest of the unwanted 1.1% of positrons, 0.8% of which are beyond the DR transverse acceptance.

3.2 Tracking with magnet errors and orbit corrections

Magnet field errors and other machine imperfections, such as misalignments which can be expressed equivalent to field errors, are randomly spread along the beamline. These errors can perturb beam orbits and beam size, and may affect beam performance. Tracking with typical magnet errors listed in Table II shows that the number of the captured positrons within the DR acceptance is only 40.2% of positrons from the target without orbit correction. The orbit perturbation explicitly makes the transverse phase spaces of some positrons beyond the DR acceptance and eats up the physical apertures, and thus the perturbed orbit needs to be corrected. The correctors should be positioned near the maximum values of β-function in the corresponding plane to efficiently correct

the orbit. In other words, one horizontal corrector is placed near a focusing quadrupole while one vertical corrector near a defocusing quadrupole. After the orbit correction, 49.8% of positrons are captured within the 6-D acceptance. We tested different random seeds of magnet errors, and the results are similar. Fig. 15 shows the transverse phase spaces at the entrance of DR injection line without errors, with errors but without orbit correction, and with errors and orbit correction. It shows that the orbit is properly corrected. Comparisons of the capture efficiency for different conditions are summarized in Table III.

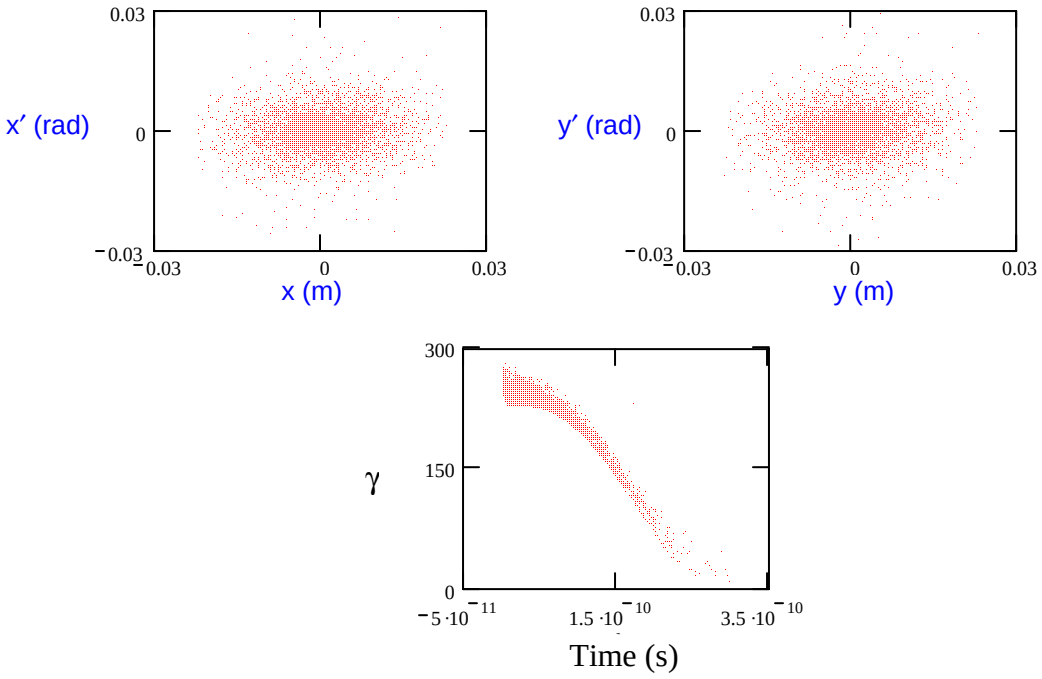

FIG. 11. Input 6-D phase spaces at the PCAP.

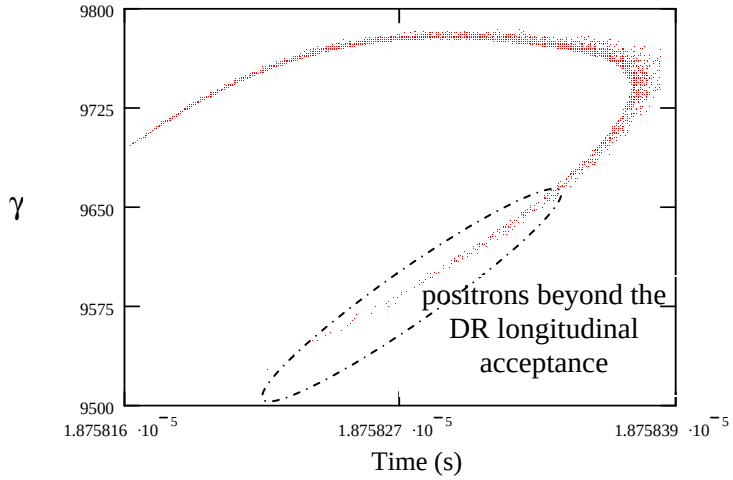

FIG. 12. Longitudinal phase space at the PLTR including energy compression without collimation.

TABLE I. Preliminary definition for physical apertures along the beamline.

Components	Half aperture in x/y (cm)
Capture cavities	2.3/2.3
PCAP	7.5/7.5
PPA	2.3/2.3
PPATEL	7.5/7.5
PTRAN	7.5/7.5
PBSTR	3.7/3.7
PLTR	
RF section	3.7/3.7
solenoid	2.0/2.0
others	7.5/3.5

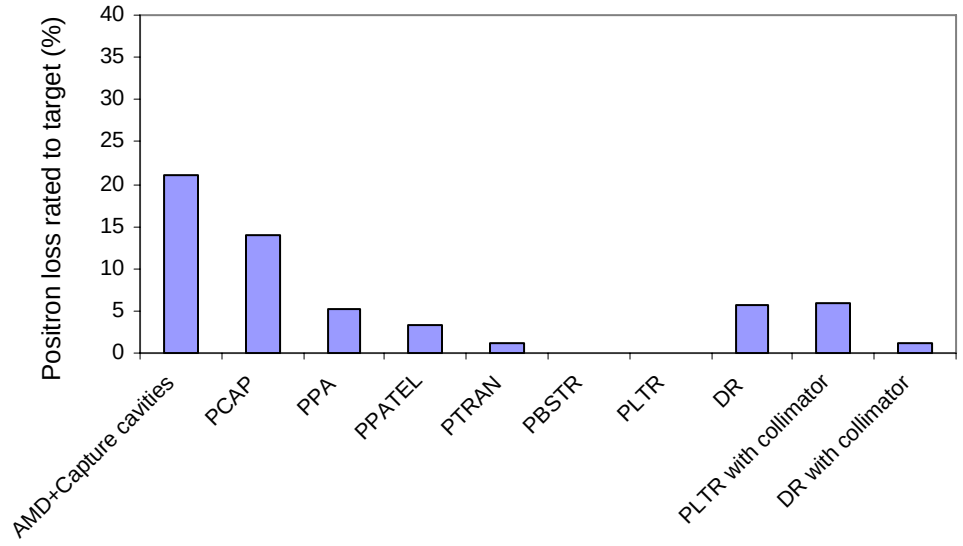

FIG. 13. Positron loss along the beamline: all positron losses are normalized to positrons at the target; when installing an energy collimator at the PLTR, the loss at the DR is reduced to 1.1%.

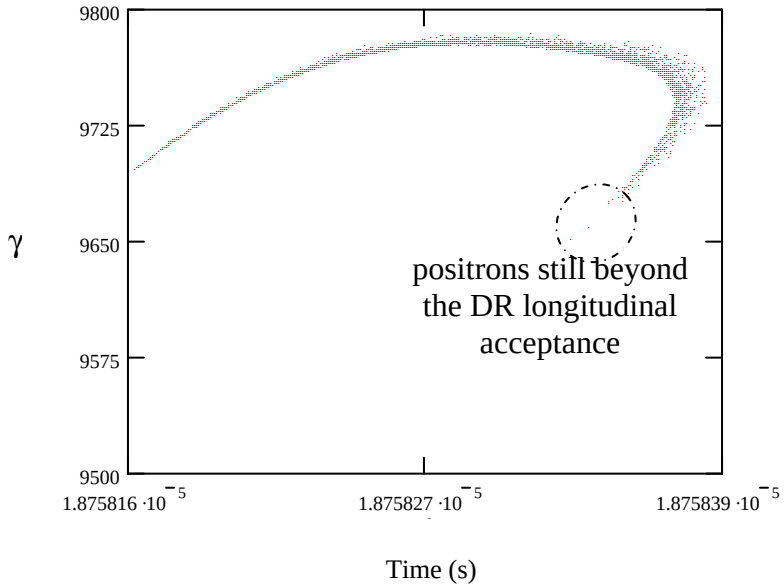

FIG. 14. Longitudinal phase space at the DR injection line with an energy collimator installed at the PLTR; positrons within the dash circle are beyond the DR 6-D acceptance.

TABLE II. RMS values of magnet errors used for tracking.

	Misalignment in x and y plane	Field error	Rotation error
Quad	$\Delta x = 200\ \mu m$ $\Delta y = 200\ \mu m$	0.1%	
Sextupole	$\Delta x = 200\ \mu m$ $\Delta y = 200\ \mu m$	0.1%	
Bend	$\Delta x = 200\ \mu m$ $\Delta y = 200\ \mu m$	0.1%	0.3 mrad

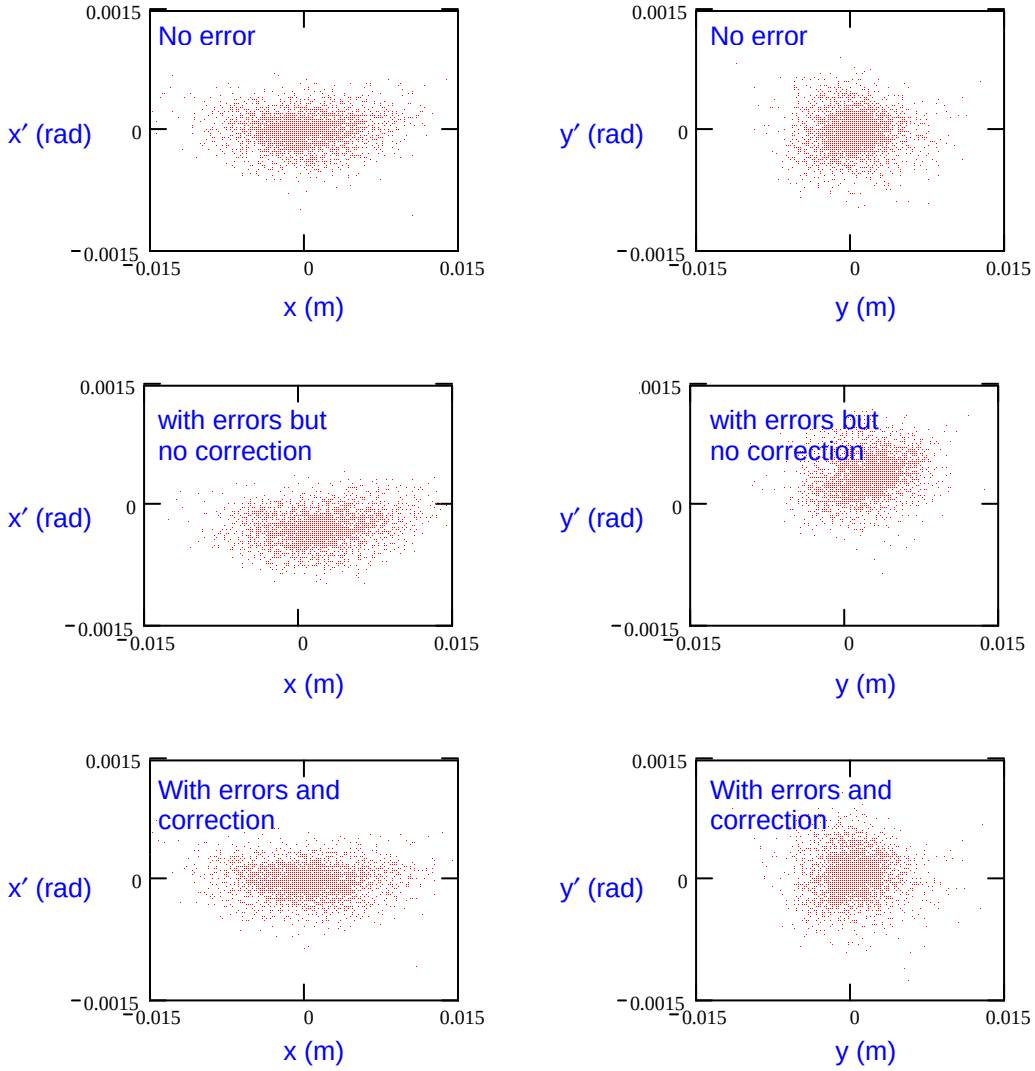

FIG. 15. Transverse phase spaces at the DR injection line without magnet errors, with errors but without correction, and with errors and correction.

TABLE III. Comparison of capture efficiency for different cases.

	Survived in physical aperture	Captured within DR Trans. acceptance	Captured within DR 6-D acceptance
Without magnet errors	55.4%	53.3%	49.8%
Without errors and with collimation in the PLTR	49.6%	48.8%	48.5%
With errors without orbit correction	54.9%	42.8%	40.2%
With errors but with orbit correction	55.4%	53.0%	49.8%

4. Summary and future work

Start-to-end beam optics for the ILC undulator-based positron source is developed; complete multi-particle tracking from the immersed Ti target with thickness of 0.4 radiation length to the entrance of DR injection line without and with magnet errors, is performed. The tracking shows that 49.8% of positrons from the target are captured within DR 6-D acceptance at the entrance of the DR injection line. Orbit perturbations caused by magnet errors along the beamline are corrected.

Looking towards the Engineering Design Report for the real construction, a lot more detail work is needed including: (1) full beamline optics and physical aperture optimizations to meet the engineering design; (2) reducing beyond-DR-acceptance positrons getting into DR by extensively optimizing both betatron and energy collimators in the PLTR; (3) start-to-end tracking as parameters of undulator and/or target changes; (4) modeling of the activation in the 5-GeV collimators; (5) component tolerances definition; and (5) defining tuning requirements.

Acknowledgement

F. Zhou would like to thank M. Borland for his great help and discussions on properly using Elegant code to track the unique positron beam. He also thanks V. Bharadwaj, N. Phinney, and T. Raubenheimer for the helpful discussions and encouragements. Work is supported by DOE contract DE-AC02-76SF00515.

References

1. TESLA TDR, DESY 2001-011, DESY, 2001.
2. Y. Batygin, “Analysis of positron collection in the linear collider”, PAC’05, Knoxville, 2005.
3. Y. Nosochkov, http://www.slac.stanford.edu/~yuri/ILC/
4. J. Wang, *et al.*, “Studies of room temperature accelerator structures for the ILC positron source”, PAC’05, Knoxville, 2005.
5. F. Zhou, *et al.*, “Preliminary beam optics for the ILC e+ source”, unpublished, 2006.
6. M. Woodley, private communication, 2006.
7. I. Reichel, private communication, 2006.
8. D. Walz, 2nd ILC accelerator workshop, Snowmass, Aug. 14-27, 2005.
9. M. Borland, Technical Report No. LS-287, ANL, 2000.
10. A. Wolski, private communication, Nov. 2006.